

INVITED PAPER

Modulation Transfer Function of Infrared Focal Plane Arrays

S. D. Gunapala, S. B. Rafol, D. Z. Ting, A. Soibel, C. J. Hill, A. Khoshakhlagh, J. K. Liu, J. M. Mumolo, S. A. Keo, L. Höglund, and E. M. Luong

Center for Infrared Photodetectors, Jet Propulsion Laboratory, California Institute of Technology, 4800 Oak Grove Drive, Pasadena, CA 91109

ABSTRACT

Modulation transfer function (MTF) is the ability of an imaging system to faithfully image a given object. The MTF of an imaging system quantifies the ability of the system to resolve or transfer spatial frequencies. In this presentation we will discuss the detail MTF measurements of 1024x1024 pixels mid-wavelength and long-wavelength quantum well infrared photodetector, and 320x256 pixels long-wavelength InAs/GaSb superlattice infrared focal plane arrays (FPAs). Long wavelength Complementary Barrier Infrared Detector (CBIRD) based on InAs/GaSb superlattice material is hybridized to recently designed and fabricated 320x256 pixel format ROIC. The n-type CBIRD was characterized in terms of performance and thermal stability. The experimentally measured NE Δ T of the 8.8 μ m cutoff n-CBIRD FPA was 18.6 mK with 300 K background and f/2 cold stop at 78K FPA operating temperature. The horizontal and vertical MTFs of this pixel fully delineated CBIRD FPA at Nyquist frequency are 49% and 52%, respectively.

Keywords: modulation transfer function, Infrared, focal planes, QWIP, superlattice, long-wave infrared

1. INTRODUCTION

Fast Fourier transformation of a spatial impulse response of an electro-optical imaging system provides the optical transfer function or the modulation transfer function (MTF) of the system in the spatial frequency domain. The MTFs of the sub-systems in the spatial frequency domain could be multiplied to get the overall MTF of an imaging system. This is much more convenient than the repeated convolutions that would be required for a spatial domain analysis, and it produces a quick understanding of the performance limitations of the overall system in terms of individual subsystems in the complete system. MTF is the ability of an imaging system to faithfully image a given object. The MTF of an imaging system quantifies the ability of the system to resolve or transfer spatial frequencies [1]. Consider a bar pattern with a cross-section of each bar being a sine wave. Since the image of a sine wave light distribution is always a sine wave, the image is always a sine wave independent of the other effects in the imaging system such as aberration. Usually, imaging systems don't have any difficulty in reproducing a bar pattern when the bar pattern is closely spaced. However, an imaging system reaches its limit when the features of a bar pattern get closer and closer together. A quantity modulation (M) for a linear, shift-invariant, and high signal-to-noise system is defined as,

$$M = \frac{E_{\max} - E_{\min}}{E_{\max} + E_{\min}},$$

where E is the irradiance. Modulation M goes to zero when ($E_{\max}-E_{\min}$) goes to zero which means there is no detectable signal above the noise floor of the system. On the other hand modulation depth approaches its maximum value of unity when E_{\min} goes to zero, which represents an ideal imaging system. Once the modulation of an image is measured experimentally, the MTF of imaging system can be calculated for that spatial frequency, using,

$$MTF = \frac{M_{\text{image}}}{M_{\text{object}}}.$$

Generally, MTF is measured over a range of spatial frequencies using a series of bar pattern targets. It is also customary to work in the frequency domain rather than the spatial domain [2]. This is done using a fast Fourier

transform (FFT) of the digitally recorded image. The absolute value of the FFT of the point spread function is then squared to yield the power spectral density of the image, S_{image} . The MTF can be calculated using,

$$MTF = \sqrt{\frac{S_{image}}{S_{object}}}$$

The approach we have taken to measure the MTF of an electro-optical system is by imaging a knife-edge target along the horizontal and vertical orientations. Fig. 1 shows how a slightly tilted knife-edge could be imaged at the pixelated focal plane arrays (FPAs).

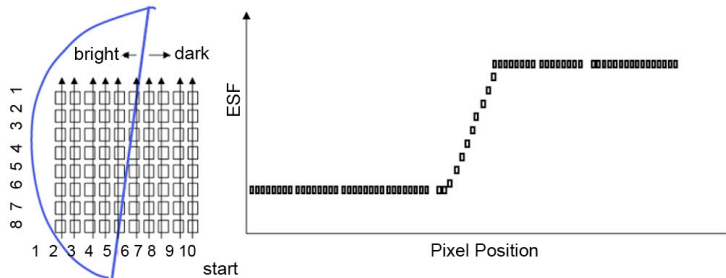


Fig. 1. This figure shows a construction of an edge-spread-function (ESF) from a selected region-of-interest (ROI) of an image.

The edge spread function (ESF) is constructed by selecting a region of interest (ROI) that intersects the knife-edge image. The ROI on Fig. 1 has 10 columns and 8 rows. The ESF could be constructed by plotting the signal strength of pixels starting from the lower right and continue towards the direction indicated by the arrow. When it reaches the top of column 9, continue the plotting process from row 8 and column 9. It ends at row 1 and column 1. The advantage of this approach is that it preserves the correlation of the data points except the end points where it can create discontinuity [3]. By properly choosing the number of rows and columns, one can construct roughly a continuous (smooth) edge spread function [4-5]. One can equally start from the upper left hand corner (i.e., row 1 and column 1) and ends up at the right bottom (i.e., row 8 and column 10). This will also give an ESF, but starts with high signal pixels on the left and ends up with low signal pixels on the right (i.e., inverse of the right side of Fig. 1). Figure 2(a) shows a ROI of an actual image of a knife-edge. Figure 2(b) shows the ESF constructed from this image using 735 data points.

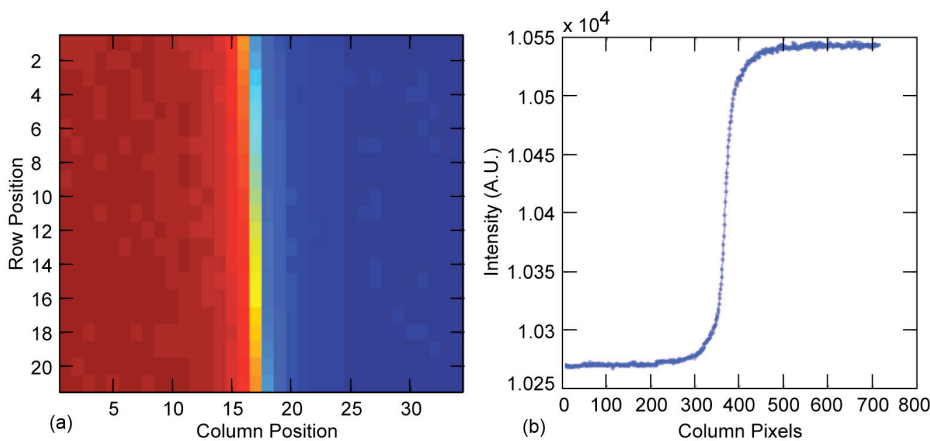


Fig. 2. (a) ROI of an image of slightly tilted knife-edge; (b) ESF constructed from the data in Fig. 2(a).

The ESF is numerically differentiated to obtain the Line Spread Function (LSF). Figure 3(a) shows the LSF corresponding to the image shown in Fig. 2(a). The zero frequency normalized absolute value of the Fourier transform

of the LSF is the one dimensional MTF of the system and Fig. 3(b) shows the MTF as a function of spatial frequency which corresponds to the image in Fig. 2(a).

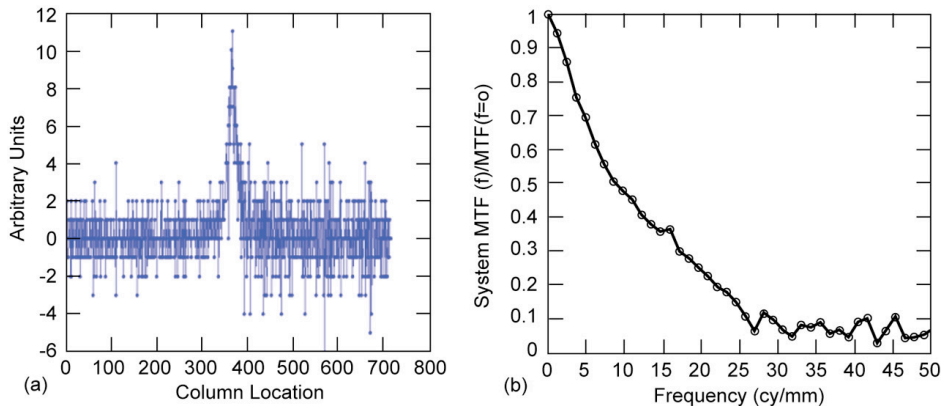


Fig. 3. (a) The line-spread-function (LSF) associated with Fig. 2(b); (b) Modulation transfer function (MTF) of the FPA which produced the image shown in Fig. 2(a).

The MTF of optical assembly could be removed by dividing the measured total MTF of the aggregate system with the MTF of optical assembly. This provides the upper limit for the FPA MTF assuming that there is no MTF loss due to the electronics, analog-to-digital conversion process, display, connecting cables, etc.

2. MID-WAVELENGTH INFRARED QWIP DEVICE

A quantum well structure designed to detect infrared (IR) light is commonly referred to as a quantum well infrared photodetector (QWIP [6-7]). A coupled-quantum well structure was used in this device to broaden the responsivity spectrum. In the MWIR device described here, each period of the multi-quantum-well (MQW) structure consists of coupled quantum wells of 40 Å containing 10 Å GaAs, 20 Å $\text{In}_{0.3}\text{Ga}_{0.7}\text{As}$, and 10 Å GaAs layers (doped $n = 1 \times 10^{18} \text{ cm}^{-3}$) and a 40 Å undoped barrier of $\text{Al}_{0.3}\text{Ga}_{0.7}\text{As}$ between coupled quantum wells, and a 400 Å thick undoped barrier of $\text{Al}_{0.3}\text{Ga}_{0.7}\text{As}$. Stacking many identical periods (typically 50) together increases photon absorption. Ground state electrons are provided in the detector by doping the GaAs well layers with Si. This photosensitive MQW structure is sandwiched between 0.5 μm GaAs top and bottom contact layers doped $n = 5 \times 10^{17} \text{ cm}^{-3}$, grown on a semi-insulating GaAs substrate by molecular beam epitaxy (MBE). Then a 0.7 μm thick GaAs cap layer on top of a 300 Å $\text{Al}_{0.3}\text{Ga}_{0.7}\text{As}$ stop-etch layer was grown *in situ* on top of the device structure to fabricate the light coupling optical cavity [7].

The experimentally measured peak absorption (or internal) quantum efficiency (η_a) of this material at room temperature was 19%. Due to the fact that the n-i-n QWIP device is a photoconductive device, the net (or external) quantum efficiency η can be determined using $\eta = \eta_a \cdot g$, where g is the photoconductive gain of the detector. The epitaxially grown material was processed into 200 μm diameter mesa test structures (area = $3.14 \times 10^{-4} \text{ cm}^2$) using wet chemical etching, and Au/Ge ohmic contacts were evaporated onto the top and bottom contact layers. The detectors were back illuminated through a 45° polished facet [6] and a responsivity spectrum is shown in Fig. 4. The responsivity of the detector peaks at 4.6 μm and the peak responsivity (R_p) of the detector is 170 mA/W at bias $V_B = -1 \text{ V}$. The spectral width and the cutoff wavelength are $\Delta\lambda/\lambda = 15\%$ and $\lambda_c = 5.1 \text{ μm}$ respectively. The photoconductive gain, g , was experimentally determined using [6] $g = i_n^2 / 4eI_D B + 1/2N$, where B is the measurement bandwidth, N is the number of quantum wells, and i_n is the current noise, which was measured using a spectrum analyzer. The photoconductive gain of the detector was 0.23 at $V_B = -1 \text{ V}$ and reached 0.98 at $V_B = -5 \text{ V}$. Since the gain of a QWIP is inversely proportional to the number of quantum wells N , the better comparison would be the well capture probability p_c , which is directly related to the gain [6] by $g = 1/Np_c$. The calculated well capture probabilities are 25% at low bias (i.e., $V_B = -1 \text{ V}$) and 2% at high bias (i.e., $V_B = -5 \text{ V}$), which together indicate the excellent hot-electron transport in this device structure. The peak net quantum efficiency was determined using $\eta = \eta_a \cdot g$. Thus, the net peak

quantum efficiency at bias $V_B = -1V$ is 4.6%. The peak detectivity is defined as $D_p^* = R_p \sqrt{AB} / i_n$, where R_p is the peak responsivity, A is the area of the detector and $A = 3.14 \times 10^{-4} \text{ cm}^2$. The measured peak detectivity at bias $V_B = -1V$ and temperature $T = 90 \text{ K}$ is $4 \times 10^{11} \text{ cm} \sqrt{\text{Hz}} / \text{W}$. Fig. 5 shows the peak detectivity as a function of detector operating temperature at bias $V_B = -1V$. These detectors show BLIP at a bias $V_B = -1V$ and temperature $T = 90 \text{ K}$ for 300 K background with $f/2.5$ optics.

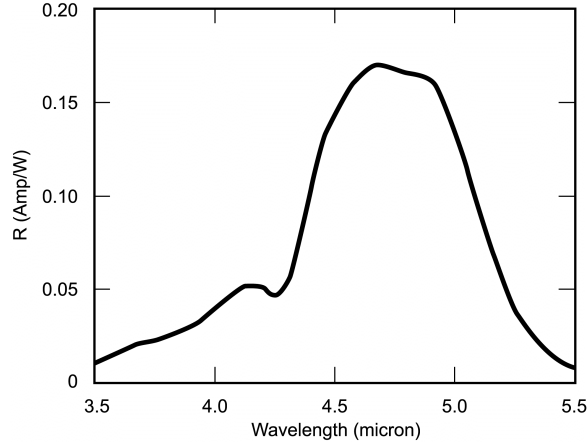


Fig 4. Responsivity spectrum of a bound-to-quasibound MWIR QWIP test structure at temperature $T = 77 \text{ K}$. The spectral response peak is at $4.6 \mu\text{m}$ and the long wavelength cutoff is at $5.1 \mu\text{m}$.

3. MTF OF MEGAPIXEL MWIR QWIP FOCAL PLANE ARRAY

After the two-dimensional grating array was defined by lithography and dry etching, the photoconductive QWIPs of the 1024×1024 FPAs were fabricated by dry chemical etching through the photosensitive GaAs/ $\text{Al}_x\text{Ga}_{1-x}\text{As}$ MQW layers into the $0.5 \mu\text{m}$ thick doped GaAs bottom contact layer. The pitch of the FPA is $19.5 \mu\text{m}$ and the actual pixel size is $17.5 \times 17.5 \mu\text{m}^2$. The two-dimensional gratings on top of the detectors were then covered with Au/Ge and Au for Ohmic contacts and high reflectivity. A few QWIP FPAs were chosen and hybridized (via an indium bump-bonding process) to a 1024×1024 silicon CMOS ROICs and biased at $V_B = -1V$. At temperatures below 90 K , the signal to noise ratio of the system is limited by array non-uniformity, ROIC readout noise, and photo current (photon flux) noise. At temperatures above 90 K , temporal noise due to the QWIP's higher dark current becomes the limitation. Fig. 5 shows the detectivity D^* as a function of device operating temperature.

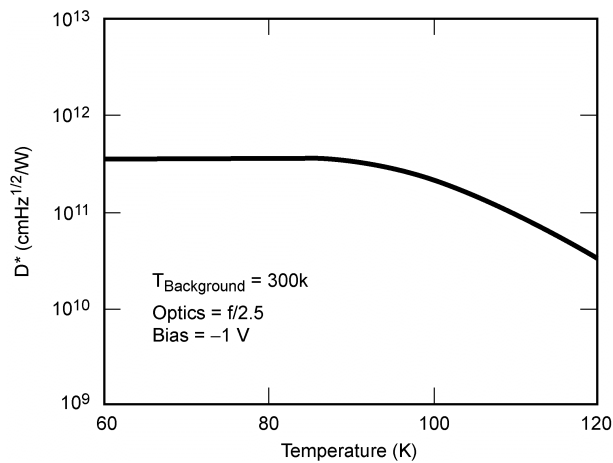


Fig 5. Detectivity as a function of detector operating temperature at bias of $V_B = -1V$.

We have used the following equation to calculate the noise equivalent differential temperature NEAT of the FPA:

$$NE\Delta T = \frac{\sqrt{AB}}{D_B^* (dP_B / dT) \sin^2(\theta / 2)}$$

where D_B^* is the blackbody detectivity, dP_B/dT is the derivative of the integrated blackbody power with respect to temperature, and θ is the field of view angle [i.e., $\sin^2(\theta/2) = (4f^2+1)^{-1}$, where f is the f number of the optical system]. Fig. 6 shows the NEAT of the FPA estimated from test structure data as a function of temperature for bias voltages $V_B = -1$ V. The background temperature $T_B = 300$ K, the area of the pixel $A = (17.5 \times 17.5 \mu\text{m}^2)$, the f number of the optical system is 2.5, and the frame rate is 10 Hz. Fig. 6 shows the measured NEAT of the imaging system at an operating temperature of $T = 90$ K, 60 msec integration time, bias $V_B = -1$ V for 300 K background with $f/2.5$ optics and the mean value is 23 mK. A 1024x1024 QWIP FPA hybrid was mounted onto a 5 W integral Sterling closed-cycle cooler assembly to demonstrate a portable MWIR camera. The digital acquisition resolution of the camera is 14-bits, which determines the instantaneous dynamic range of the camera (i.e., 16,384). The preliminary data taken from a test set up has shown mean system NEAT of 22 mK (the higher NEAT is due to the 65% transmission through the lens assembly, and system noise of the measurement setup) at an operating temperature of $T = 90$ K and bias $V_B = -1$ V, for a 300 K background. Video images were taken at a frame rate of 10 Hz at temperatures as high as $T = 90$ K, using a ROIC capacitor having a charge capacity of 8×10^6 electrons (the maximum number of photoelectrons and dark electrons that can be counted in the time taken to read each detector pixel). Fig. 7(a) shows one frame of a video image taken with a 5.1 μm cutoff 1024x1024 pixel QWIP camera.

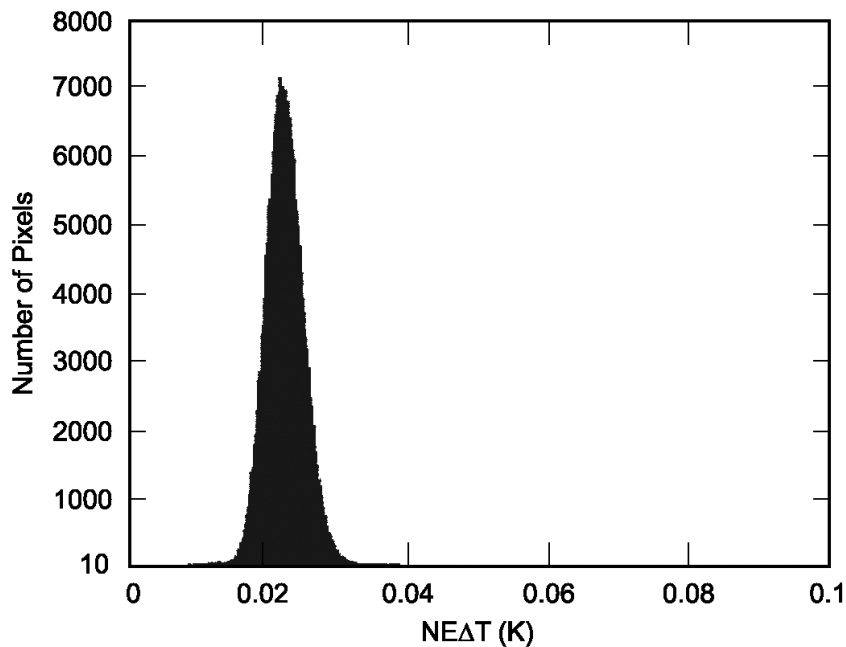


Fig 6. NEAT histogram of the 1,048,576 pixels of the 1024x1024 array showing a high uniformity of the FPA.

Fig. 7(b) shows the MTF of the imaging system as a function of spatial frequency. It is important to remember that the MTF of a system is a property of the entire system, therefore, all of the system components such as the FPA, lens assembly, cabling, framegrabber, cooler, A/D converter, etc. contribute to the final MTF performance of the system. The MTF of the optics at Nyquist frequency is 0.2, thus the MTF of the FPA should be 30% and 45% at the Nyquist frequency $N_y = 25.6$ Cy/mm ($N_y = 1/2 \cdot \text{pixel pitch}$) along horizontal and vertical axes, respectively. Higher MTF at Nyquist indicates that QWIP FPA has the ability to detect smaller targets at large distances since optical and electronic energy are not spread among adjacent pixels. It is already shown elsewhere the MTF of a perfect FPA (i.e., no pixel-to-pixel cross-talk) is 0.64 at the Nyquist frequency. In other words, this data shows that the pixel-to-pixel cross-talk (optical and electrical) of MWIR megapixel FPA is almost negligible at Nyquist. This was to be expected, because this

FPA was back-illuminated through the flat thinned substrate membrane (thickness $\approx 800 \text{ \AA}$). This substrate thinning (or removal) should completely eliminate the pixel-to-pixel optical cross-talk of the FPA. In addition, this thinned GaAs FPA membrane has completely eliminated the thermal mismatch between the silicon CMOS ROIC and the GaAs based QWIP FPA. Basically, the thinned GaAs based QWIP FPA membrane adapts to the thermal expansion and contraction coefficients of the silicon ROIC. For these reasons, thinning has played an extremely important role in the fabrication of large area FPA hybrids.

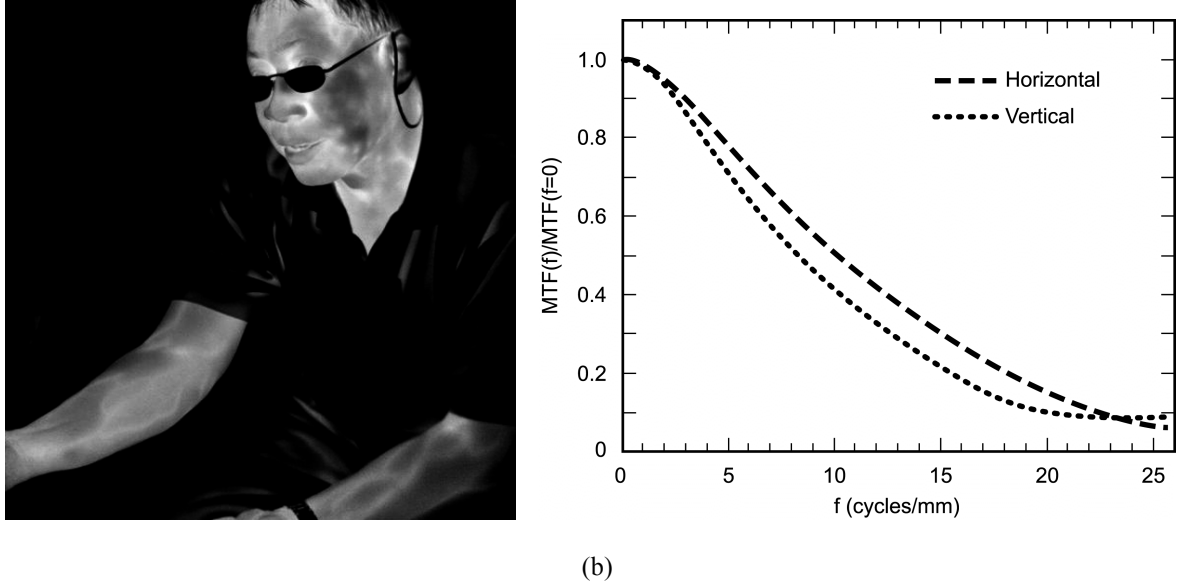


Fig 7. (a) Picture a 1024x1024 pixel QWIP focal plane array mounted on a 84-pin lead less chip carrier; (b) Horizontal and vertical MTF of the MWIR imaging system based on a 1024x1024 pixel QWIP MWIR camera.

4. LONG-WAVELENGTH INFRARED QWIP DEVICE

Each period of this LWIR MQW structure consists of quantum wells of 40 \AA and a 600 \AA barrier of $\text{Al}_{0.27}\text{Ga}_{0.73}\text{As}$. As mentioned earlier, stacking many identical periods (the device in this study has 50 periods) together increases photon absorption. Ground state electrons are provided in the detector by doping the GaAs well layers with silicon impurities up to $n = 5 \times 10^{17} \text{ cm}^{-3}$. This photosensitive MQW structure is sandwiched between 0.5 \mu m GaAs top and bottom contact layers doped $n = 5 \times 10^{17} \text{ cm}^{-3}$, grown on a semi-insulating GaAs substrate by MBE. Then a 0.7 \mu m thick GaAs cap layer on top of a 300 \AA $\text{Al}_{0.27}\text{Ga}_{0.73}\text{As}$ stop-etch layer was grown *in situ* on top of the device structure to fabricate the light coupling optical cavity. The MBE grown material was tested for absorption efficiency using a FTIR spectrometer. Test detectors with a 200 \mu m diameter were fabricated and back-illuminated through a 45° polished facet for optical characterization and an experimentally measured responsivity spectrum is shown in Fig. 8(a). The responsivity of the detector peaks at 8.4 \mu m and the peak responsivity (R_p) of the detector is 130 mA/W at bias $V_B = -1 \text{ V}$. The spectral width and the cutoff wavelength are $\Delta\lambda/\lambda = 10\%$ and $\lambda_c = 8.8 \text{ \mu m}$, respectively. The photoconductive gain g was experimentally determined as described in the previous section. The peak detectivity of the LWIR detector was calculated using experimentally measured noise current i_n . The calculated peak detectivity at bias $V_B = -1 \text{ V}$ and temperature $T = 70 \text{ K}$ is $1 \times 10^{11} \text{ cm} \sqrt{\text{Hz}} / \text{W}$ (see Fig. 8(b)). These detectors show BLIP at bias $V_B = -1 \text{ V}$ and temperature $T = 72 \text{ K}$ for a 300 K background with $f/2.5$ optics.

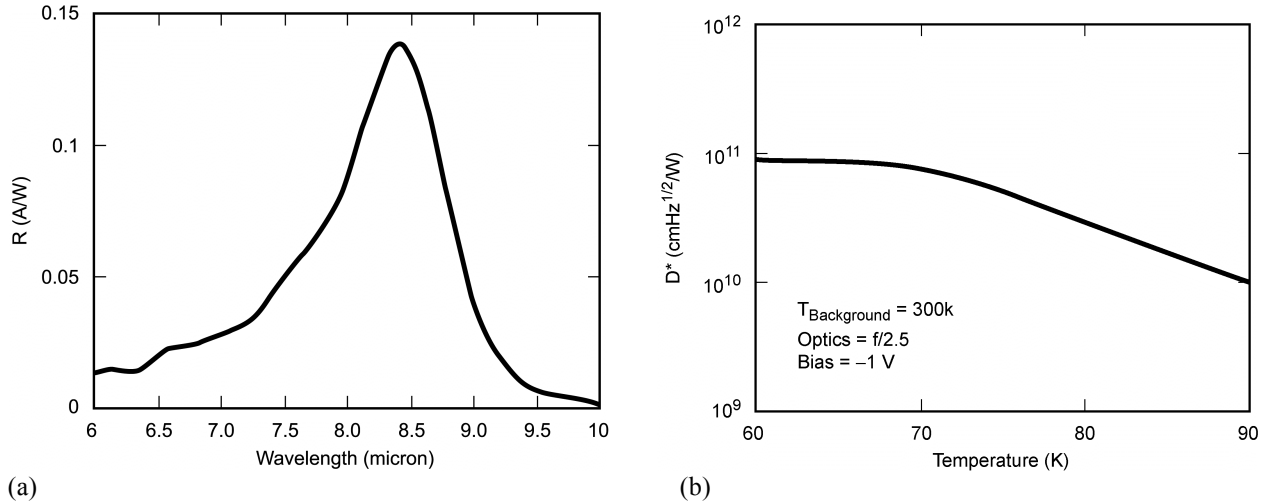


Fig 8. (a) Responsivity spectrum of a bound-to-quasibound LWIR QWIP test structure at temperature $T = 77$ K. The spectral response peak is at $8.4 \mu\text{m}$ and the long wavelength cutoff is at $8.8 \mu\text{m}$; (b) detectivity as a function of temperatures at bias of -1 V.

5. MTF OF MEGAPIXEL LWIR QWIP FOCAL PLANE ARRAY

A megapixel LWIR QWIP detector arrays were fabricated as described earlier. The pitch of the FPA is $19.5 \mu\text{m}$ and the actual pixel size is $17.5 \times 17.5 \mu\text{m}^2$. The two-dimensional gratings on top of the detectors were then covered with Au/Ge and Au for Ohmic contacts and high reflectivity. Nine 1024×1024 pixel QWIP FPAs were processed on a 4-inch GaAs wafer. Indium bumps were then evaporated on top of the detectors for hybridization with silicon CMOS ROICs. A single QWIP FPA was chosen and hybridized (via indium bump-bonding process) to a 1024×1024 CMOS multiplexer and biased at $V_B = -1$ V. At temperatures below 72 K, the signal-to-noise ratio of the system is limited by array nonuniformity, ROIC readout noise, and photocurrent (photon flux) noise. At temperatures above 72 K, the temporal noise due to the dark current becomes the limitation. The differential resistance R_{Det} of the pixels at -1 V bias is 7.4×10^{10} Ohms at $T = 70$ K and detector capacitance C_{Det} is 1.7×10^{-14} F. The detector dark current $I_{\text{Det}} = 1.6$ pA under the same operating conditions. This initial array gave excellent images with 99.98% of the pixels working (number of dead pixels ≈ 200), again demonstrating the high yield of GaAs technology.

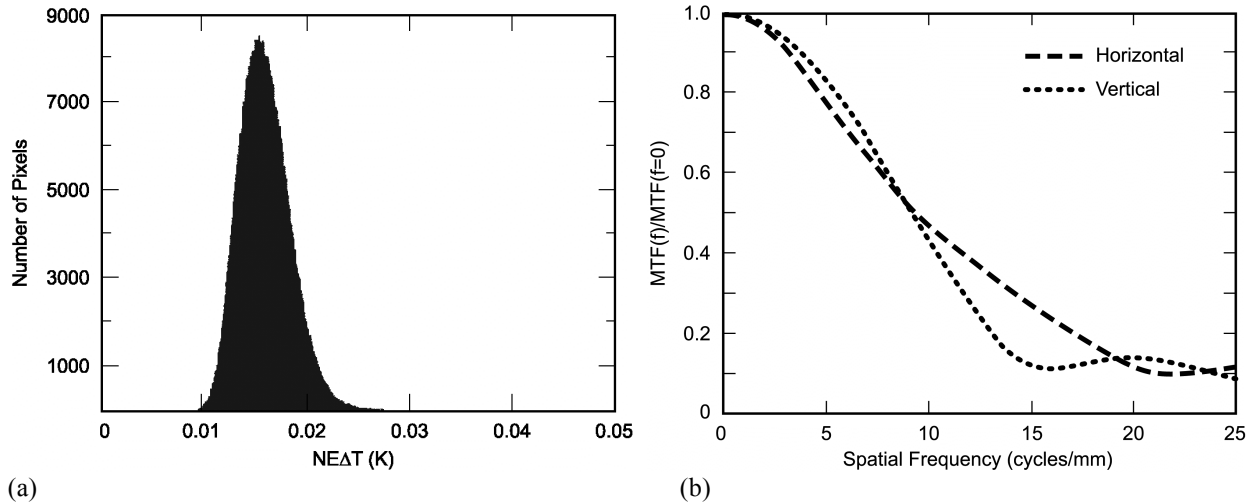


Fig 9. (a) NEAT histogram of the megapixel LWIR QWIP FPA showing a high uniformity of the FPA. The uncorrected non-uniformity As shown in this figure, after single-point correction non-uniformity reduced to 0.8% ; (b) horizontal and vertical MTF of the MWIR imaging system based on a 1024×1024 pixel QWIP MWIR camera.

NEAT of the FPA was calculated as described earlier. Fig. 9(a) shows the measured NEAT of the system at an operating temperature of $T = 72\text{K}$, 29 msec integration time, bias $V_B = -1\text{V}$ for 300K background with $f/2.5$ optics and the mean value is 16mK. Fig. 9(b) shows the MTF of the imaging system as a function of spatial frequency. The MTF of the spot scanner optics at Nyquist frequency is 0.2, thus the MTF of the FPA should be > 0.5 at the Nyquist frequency $N_y = 25.6\text{ Cy/mm}$. As mentioned earlier, the MTF of an ideal FPA (i.e., no pixel to pixel cross-talk) is 64% at Nyquist frequency. Thus, the pixel to pixel optical and electrical cross-talk of this LWIR megapixel FPA is negligibly small. We have observed oscillations in many of our MTF measurements, and this may be due to the unfiltered high frequency noise on the point spread function (PSF) due to pattern noise. These oscillations become more pronounced at higher frequency when MTF approaches the noise floor. The source of high frequency is most likely the ROIC and electronics. We do not think this is temporal in origin since we have averaged 64 frames or more for the PSF measurement. At 15 Cy/mm the lens MTF is approximately 0.38, so the detector MTF at 15 Cy/mm is approximately 26.3 %. This is much less than the ideal MTF of the FPA.

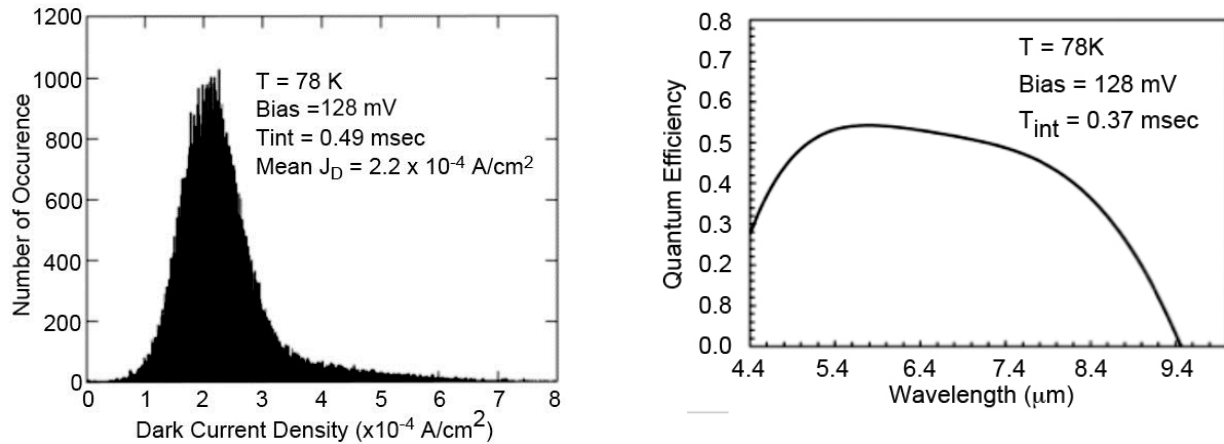
6. CBIRD DEVICE STRUCTURE

The complementary barrier infrared detector (CBIRD) structure needs n on p ROIC as an electrical interface since it provides electrons at the top contact. This CBIRD design consists of a 300-period (44 Å, 21 Å)-InAs/GaSb absorber superlattice (SL) sandwiched between an 80-period (46 Å, 12 Å)-InAs/AlSb hole-barrier (hB) SL on the left and 60-period (22 Å, 21 Å)-InAs/GaSb electro-barrier (eB) SL on the right. The hB SL and eB SL are, respectively, designed to have approximately zero conduction and valence band offset with respect to the absorber SL. The hB SL is doped at $n=1 \times 10^{16}\text{ cm}^{-3}$ while the absorber SL and eB SL are nominally doped at $p=1 \times 10^{16}\text{ cm}^{-3}$, and $p=1 \times 10^{16}\text{ cm}^{-3}$ [9-10]. InAs_{0.91}Sb_{0.09} adjacent to the eB acts as the $V_{\text{DET_COM}}$ contact layer, and the hB SL serves as the top contact layer that is electrically connected to the ROIC. For CBIRD the $V_{\text{DET_COM}}$ is at a lower potential relative to the top contact or ROIC. This injects electrons into the ROIC and the mode is n on p. The dry etching process was utilized to fabricate the 320 x 256 pixel arrays with 30 μm pixel pitch. FLIR/Indigo two-color direct injection 320x256 pixel format ISC0903 ROIC [11] was used to fabricate FPAs. The detector arrays and ROICs were hybridized using the SET FC-300 flip-chip bonder. After hybridization, the FPAs were backfilled with epoxy and cured overnight. The substrate was completely removed by mechanical lapping followed by a selective dry-etching process all the way down to the etch stop layer.

7. TESTING AND CHARACTERIZATION OF CBIRD FPA

The FPA was cooled down to 78K and 65K for data acquisition at two temperatures. Fig.10(a) depicts the dark current density histogram at an operating bias of 128 mV. The integration time was set slightly higher to 490 μsec, which should not affect the dark current estimate. The mean dark current density of $\sim 2.2 \times 10^{-4}\text{ A/cm}^2$ is a factor of 4.4 higher than the mean measured dark current from many single element devices at the same temperature and bias. Estimates show that at 240K background temperature the dark current density is comparable to photocurrent density from 298K background. The mean dark current density of the large area single element detectors at $\sim 77\text{K}$ was $\sim 5 \times 10^{-5}\text{ A/cm}^2$. The FPA detector array is not passivated and surface conduction may have contributed to the increase in dark current density.

Fig. 10(b) shows the plot of mean external QE as a function of wavelength, which is measured directly from the FPA at 78K, 128 mV bias, and 370 μsec integration time. The maximum QE of 54 % has been achieved for double pass geometry. This is slightly lower than the single element result. The FPA is back illuminated while the single element test device is front-illuminated. The substrate was completely removed and thinned enough to be transparent for IR radiation. The cut-off wavelength is about 8.8 μm, which is at 50% of the peak, and the Full-Width-Half-Maximum (FWHM) is from roughly from 4.4 μm to 8.8 μm. The mean responsivity is 46.2 nV/photon with operability of 97%. The operability is defined as those pixels with responsivity between 20% and 150% of the mean responsivity. The low responsivity can be partially attributed to low ROIC gain which is $\sim 97\text{ nV/electron}$ [10].



(a) (b)
Fig. 10. (a) Dark current of CBIRD at a bias of 128 mV and 78K operating temperature; (b) quantum efficiency spectrum of long-wavelength superlattice CBIRD device. Quantum efficiency was measured with double-pass geometry.

Excess dark current normally originates from generation-recombination, trap assisted tunneling, and surface leakage [8]. However, when the temperature was lowered to 65K, the mean dark current density decreased to $1.1 \times 10^{-4} \text{ A/cm}^2$. This implies that there is a surface leakage in addition to the bulk current. However, the bulk dark current density still dominates considerably and decreases with temperature. The decreasing bulk dark current density as a function of decreasing temperature clearly indicates the absence of trap assisted tunneling assuming the surface leakage current is independent of temperature. The uncorrected spatial non-uniformity (σ/mean) at 298 K blackbody temperature is 5.5%. The temporal NEAT matrix is numerically evaluated from the relations, $\text{NEAT} = \sigma_{\text{Temporal}} \Delta T / [\text{Mean}(T_H) - \text{Mean}(T_L)]$ [6]. The matrices $\text{Mean}(T_L)$ and $\text{Mean}(T_H)$ are the means evaluated at blackbody temperatures of $T_L = 293 \text{ K}$ and $T_H = 303 \text{ K}$. The temporal noise is estimated at 298 K using 32 frames, and $\Delta T \sim 10 \text{ K}$. The experimentally measured NEAT histograms distributions of the CBIRD FPA at 78K operating temperature, 128 mV bias, and 370 μsec integration time, with blackbody temperature of 298 K and an f/2 cold stop, is shown in the Fig. 11. The mean NEAT of 18.6 mK and 12 mK is achieved at FPA operating temperatures of 78K and 65K respectively. This means that noise has decreased with temperature.

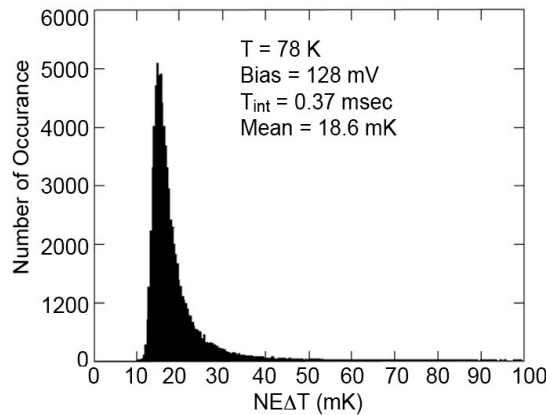


Fig. 11. Measured CBIRD NEAT histogram operating at 78K, bias of 128 mV and integration time of 370 μsec . The mean NEAT is 18.6 mK.

8. MR Δ T AND MTF OF CBIRD FPA

In this section we describe the minimum resolvable temperature difference (MR Δ T) and MTF measurements. Figure 12(a) and (b) depict MR Δ T and MTF plots of an LWIR CBIRD FPA respectively. MR Δ T is a subjective measurement of an FPA image using trained human observers. It requires a stable differential temperature between background and a four bar target that will produce a unity signal-to-noise ratio on the display monitor as a function of target spatial frequency [1]. This measures thermal sensitivity as a function of spatial resolution defined by the four bar target with aspect ratio of 7:1. The period of the four bar target is varied and the spatial frequency is estimated for each four bar target. At small spatial frequency, the horizontal MR Δ T (HMR Δ T) and vertical MR Δ T (VMR Δ T) are slightly lower than the NE Δ T value, which is also shown on the MR Δ T plot. At higher spatial frequency, it requires a larger temperature difference to generate a contrast between the four bar targets and background. Positive and negative contrast was measured and temperature difference was averaged to eliminate the offset. The four bar target becomes difficult to resolve at 15.89 cycles/mm (which is just below Nyquist frequency \sim 16.67cycles/mm) in both the vertical and horizontal direction even after moving the target slightly to compensate for the phasing effect and raising the temperature of the background [3]. It is observed that only three bars were apparent instead of four and two of the bars merge into one at a frequency close to Nyquist.

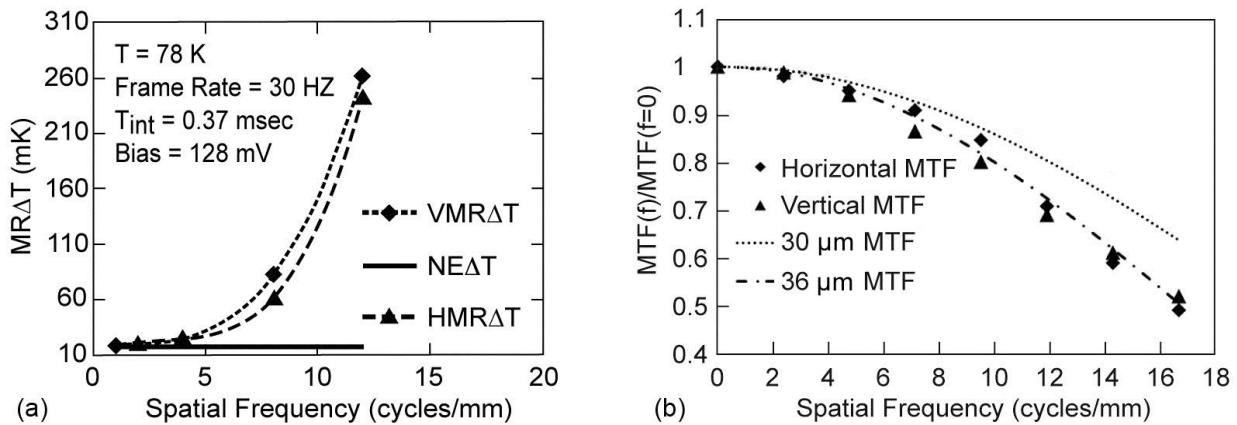


Fig. 12. (a) Minimum Resolvable Temperature Difference (MR Δ T) and (b) Modulation Transfer Function (MTF) as a function of spatial frequency measured from 320 x 256 CBIRD FPA operating at 78K, at a bias at 128 mV and integration time of 370 μ sec.

MTF technically provides a measure of image resolution or spatial frequency response of the infrared imaging system. It is a measure of how the contrast is transferred from object space to image space as a function of spatial frequency. MTF is inversely related to MR Δ T [8]. The ESF is then constructed as previously described. The ESF is numerically differentiated to obtain the LSF. The zero frequency normalized absolute value of the Fourier transform of the LSF is the one dimensional MTF of the system. The lens MTF is removed by dividing the measured MTF with the lens MTF. The plot in Figure 12(b) is MTF(f)/MTF(f=0) of the FPA and electronics in horizontal and vertical orientation.

The higher MTF at low frequency produces better contrast (see Fig. 13) and, therefore better images are observed at low spatial frequency. Higher MTF values at high frequency produce good quality images at higher frequency. The horizontal and vertical MTFs at Nyquist frequency based on pixel pitch, a , ($= 1/2a$, $a = 30\mu\text{m}$) \sim 16.67cycles/mm are about \sim 0.49 and \sim 0.52, respectively. The Nyquist frequency is well below the optical cut off frequency of \sim 56.8 cycles/mm based on the 8.8 μm detector cut off wavelength. The loss of MTF can be due to defocusing [4-5, 8] and this defocusing effect is eliminated by acquiring data at the best focus and then collecting data by moving the FPA by $\pm 50 \mu\text{m}$ along the optical axis from the best focus location. This 50 μm move is roughly the size of the Airy disk. The FPA MTF can be separated into the product of two components. The geometric aperture MTF is related to the pixel size and the diffusion MTF related to electro-optical properties [1-5]. The diffusion MTF depends on the diffusion length and geometry. The carrier diffusion degrades high frequency MTF and manifests as crosstalk (or MTF loss).

However, the CBIRD pixels are delineated down to the bottom contact and it is expected that no lateral carrier diffusion into the next neighbor can occur. The advantage of delineation is the reduction of cross talk. The disadvantage (in non-planar device structures) is that the fill factor is less than 100%. Shorter wavelengths on the other hand can be absorbed near the top surface and can diffuse to the next neighbor. In CBIRD FPA, the only channel left for the charge carriers to diffuse to an adjacent pixel is through the thin VDET_COM layer.

The geometric aperture MTF can be estimated using a sinc function. Since the pixel is square, the aperture MTF is the same in the horizontal and vertical orientation. For a pixel pitch of $30\mu\text{m}$ (the CBIRD FPA pixel size) a sinc function describing an aperture MTF is plotted in Fig. 12(b). Smaller pixel size actually improves high frequency MTF since at Nyquist (sampling using FPA pitch) its value is greater than 0.64. The difference between aperture MTF and the measured MTF is the upper limit on the diffusion MTF (crosstalk) since other MTF components such as electronic and other effects including surface recombination are not completely understood. The ROIC crosstalk is small, $\sim 0.1\%$ by design. At Nyquist frequency, the difference between measured horizontal/vertical and the ideal MTF is ~ 0.14 , but at low frequencies the difference is small. The MTF loss is basically an effective increase of the pixel size. The geometric aperture MTF function decreases with increasing pixel size and frequency. Thus detectors can be viewed as an overlapping Gaussian-like array. For example, for horizontal and vertical MTF data in Fig. 12 the pixel size that will closely match the MTF data is roughly $\sim 36\mu\text{m}$ which is larger than the pitch. Imagery was performed at 78K FPA operating temperature and Fig. 13 shows outside natural scenery. The image quality of the natural scene attests to the very good MTF behavior at low and high frequencies. This FPA gave good images, with more than 97% of the pixels operable. Video images were taken at a frame rate of 30 Hz and integration time of 0.37 msec.



Fig. 13. Outside images taken with the long-wavelength infrared CBIRD superlattice focal plane array. The FPA is operated at 78K with NE Δ T of 18.6 mK with f/2 optics at 300K background. This image show good quality reproduction of low and high spatial frequency.

9. CONCLUSION

The MTFs of megapixel single-band and multi-band QWIP FPAs were experimentally measured. MTFs of the single-band fully pixelated MWIR and LWIR QWIP FPAs were approximately 50% including the MTF degradation due to electronics and cooler. A significant degradation of the MTF was observed in the shorter spectral bands of the nine-band QWIP FPA due to the thick underlying undelineated materials. A 320x256 format LWIR CBIRD FPA has been demonstrated with 18.6 mK NE Δ T for 300K background with f/2 cold stop at 78K FPA operating temperature. The horizontal and vertical MTFs of this pixel fully delineated CBIRD FPA at Nyquist frequency are 49% and 52%, respectively. In conclusion, the MTF measurement is a powerful and simple technique which could easily provides a measure of pixel-to-pixel cross-talk of focal plane arrays.

ACKNOWLEDGMENT

The authors thank R. Cox, R. Liang, M. Herman and E. Kolawa of JPL, and S. Bandara and M. Tidrow of the U.S. Army Night Vision Electronics Sensor Directorate. The research was carried out at the Jet Propulsion Laboratory, California Institute of Technology, under a contract with the National Aeronautics and Space Administration.

REFERENCES

- [1] G. C. Holst, *The Infrared Electro-Optical Systems Handbook*, M. C. Dudzik, Ed. Bellingham, WA: SPIE, 1993.
- [2] W. J. Smith, *Modern Optical Engineering the Design of Optical Systems*, 2nd ed. New York: McGraw-Hill, 1990.
- [3] Glenn D. Boreman, "Modulation Transfer Function in Optical and Electro-Optical Systems", SPIE Press, 2001.
- [4] Mike Davis; Mark E. Greiner; John G. Sanders; James T. Wimmers, "Resolution issues in InSb focal plane array system design", *Proc. SPIE Vol. 3379*, 1998.
- [5] H. Holloway, "Collection efficiency and crosstalk in closely spaced photodiode arrays", *J. App. Phys.* 60, pp.1091, 1998.
- [6] S. D. Gunapala, S. V. Bandara, S. B. Rafol, and D. Z. Ting, "Quantum Well Infrared Photodetectors," *Semiconductors and Semimetals*, Vol. 84, 59-151, Academic Press, 2011.
- [7] S. D. Gunapala, S. V. Bandara, J. K. Liu, C. J. Hill, S. B. Rafol, J. M. Mumolo, J. T. Trinh, M. Z. Tidrow, and P. D. LeVan, *Semicond. Sci. Technol.*, Vol. 20, pp. 473-480, 2005.
- [8] S. B. Rafol and E. Cho, "Modulation transfer function measurement on QWIP focal plane array," *SPIE Proc*, vol. 6941, pp. 69410-1-69410-12, 2008.
- [9] David Z. Ting, Cory J. Hill, Alexander Soibel, Sam A. Keo, Jason M. Mumolo, Jean Nguyen, Sarath D. Gunapala, *Appl. Phys. Lett.* Vol. 95, pp. 023508, 2009.
- [10] S. D. Gunapala, D. Z. Ting, C. J. Hill, J. Nguyen, A. Soibel, S. B. Rafol, S. A. Keo, J. M. Mumolo, M. C. Lee, J. K. Liu, and B. Yang, *IEEE Photonics Technology Letters*, Vol. 22, pp. 1856-1858, 2010.
- [11] B. Simolon, A. Aziz, R. Hansen, E. Kurth, S. Lam, S. Petronio, and J. Woolaway, *Infrared Physics & Technology*, Vol. 54, pp. 306-309, 2011.